

A Balance Equation Determines a Switch in Neuronal Excitability

Alessio Franci^{1,#}, Guillaume Drion^{2,3#}, Vincent Seutin³ & Rodolphe Sepulchre^{1,2,*}

¹INRIA Lille-Nord Europe, Orchestron project, 40 avenue Halley F 59650 Villeneuve d'Ascq, France

²Department of Electrical Engineering and Computer Science and GIGA Research, University of Liège, Liège, Belgium.

³Neurophysiology Unit, GIGA Neurosciences, University of Liège, Liège, Belgium.

#These authors contributed equally to this work.

* E-mail: R.Sepulchre@ulg.ac.be

Abstract

We use the qualitative insight of a planar neuronal phase portrait to detect an excitability switch in arbitrary conductance-based models from a simple mathematical condition. The condition expresses a balance between ion channels that provide a negative feedback at resting potential (restorative channels) and those that provide a positive feedback at resting potential (regenerative channels). Geometrically, the condition imposes a transcritical bifurcation that rules the switch of excitability through the variation of a single physiological parameter. Our analysis of six different published conductance based models always finds the transcritical bifurcation and the associated switch in excitability, which suggests that the mathematical predictions have a physiological relevance and that a same regulatory mechanism is potentially involved in the excitability and signaling of many neurons.

Author summary

Understanding the changing electrophysiological signatures of neurons in different physiological and pharmacological conditions is a central focus of experimental electrophysiology because a key component of cell signaling in the nervous system. Computational modeling may assist experimentalists in this quest by identifying core mechanisms and suggesting pharmacological targets from a mathematical analysis of the model. But a successful interplay between experiments and mathematical predictions requires new analysis tools adapted to the complexity of high-dimensional computational models nowadays available. We use bifurcation theory to propose a mathematical condition that can detect an important switch of neuronal excitability in arbitrary conductance-based neuronal models and we illustrate its physiological relevance in six published state-of-the-art models of different neurons.

Introduction

Detailed computational conductance-based models have long demonstrated their ability to faithfully reproduce the variety of electrophysiological signatures that can be recorded from a single neuron in varying physiological or pharmacological conditions. But the predictive value of a computational model is limited unless its analysis sheds light on the core mechanisms at play behind a computer simulation. Because conductance-based models are nonlinear dynamical models, their analysis often requires a drastic reduction of dimension. The reduced model is amenable to the geometric methods of dynamical systems theory, but the mathematical insight is often gained at the expense of physiological interpretability; hence the need for methodological tools that can relate mathematical predictions of low-dimensional models to physiological predictions in detailed conductance based models.

In recent work [1], we used phase plane analysis and dynamical bifurcation theory to characterize in *reduced-order* neurodynamics models a switch of excitability that is consistent with many physiological observations.

More precisely, a transcritical bifurcation governed by a single parameter was shown to organize a switch from restorative excitability, extensively studied in most models inspired from the Hodgkin-Huxley model, to regenerative excitability whose distinct electrophysiological signature include spike latency, plateau oscillations, and afterdepolarization potentials..

The main contribution of the present paper is to show that this transcritical bifurcation, and the associated excitability switch, exist in a number of *high-dimensional* conductance-based models and that the resulting mathematical predictions have physiological relevance. Although purely mathematical in nature, the detection of the transcritical bifurcation relies on an ansatz that leads to a simple physiological interpretation: the switch of excitability is determined by a balance between restorative (those providing a negative feedback) and regenerative (those providing a positive feedback) ion channels at the resting potential. Because this simple balance equation can take many different physiological forms, it is potentially shared by very different neurons.

We use the balance equation to provide an algorithm to trace the transcritical bifurcation in arbitrary conductance-based models. We apply the algorithm to detailed conductance-based models of six neurons known to exhibit drastic changes in their electrophysiological signatures depending on environmental conditions: the squid giant axon [2], the dopaminergic neuron [3], the thalamic relay neuron [4], the thalamic reticular neuron [5], the aplysia R15 model [6], and the cerebellar granular cell [7]. In each case, the algorithm identifies a transcritical bifurcation that occurs close to the nominal model parameters and its predictions are consistent with experimental observations.

After defining a novel classification of ion channels based on their restorative or regenerative nature, we briefly review the planar model presented in [1] and how its transcritical bifurcation qualitatively captures the switch between restorative and regenerative excitability. As a generalization of this low-dimensional case, we mathematically construct the same bifurcation in generic conductance based models and derive the balance condition determining the regenerative or restorative nature of the model. This construction and its electrophysiological predictions are firstly illustrated on the squid giant axon. An algorithm for generic conductance-based models is subsequently derived and different models analysed.

Results

Slow restorative and slow regenerative ion channels

Conductance-based models of neurons describe the dynamic interaction between the membrane potential V and - possibly many - gating variables that control the ionic flow through the membrane. The gating of ion channels occurs on many different timescales. However, gating timescales can be grouped in three families, according to their influence on neuronal excitability [8]:

- (i) **Fast gating variables:** These variables have a time-constant in the millisecond range. They generate the rapid regenerative upstroke of an action potential. Prominent representatives of this family are the activation gating variables of fast voltage-gated sodium channels ($\text{Na}_V1.1$ to $\text{Na}_V1.9$).
- (ii) **Slow gating variables:** These variables have a time constant 5 to 10 times larger than fast gating variables. They influence the spike initiation, downstroke, and the afterspike period. They are key players of neuronal excitability. Prominent representatives of this family are the activation gating variables of delayed rectifier potassium channels ($\text{K}_V1.1$ to $\text{K}_V1.3$, $\text{K}_V1.5$ to $\text{K}_V1.8$, $\text{K}_V2.1$, $\text{K}_V2.2$, $\text{K}_V3.1$, $\text{K}_V3.2$, $\text{K}_V7.1$ to $\text{K}_V7.5$, $\text{K}_V10.1$) and the activation gating variables of all calcium channels ($\text{Ca}_V1.x$, $\text{Ca}_V2.x$, $\text{Ca}_V3.x$).
- (iii) **Ultra-Slow (adaptation) variables:** These variables gate too slowly to be strongly activated by single action potentials. They modulate neuronal excitability only over periods of many action potentials. Prominent representative of this family are the inactivation gating variables of transient calcium channels ($\text{Ca}_V2.x$, $\text{Ca}_V3.x$). Ultra-slow variables might also include non gating variables. For instance, the intracellular calcium concentration $[\text{Ca}^{2+}]_{in}$, which modulates the conductance of calcium-regulated channels.

In view of their importance for neuronal excitability, we focus only on slow gating variables to classify ion channels: when the slow channel provides negative feedback to the membrane potential variation, we term the associated channel a slow restorative ion channel. When the slow variable instead enhances a voltage variation by positive feedback, the associated ion channel is termed slow regenerative (a characterization in

terms of partial derivatives is postponed to the next sections). Ion channels that do not possess a slow gating variable are neither restorative nor regenerative and are called neutral. Neutral ion channels solely regulate the “quantity” of excitability without affecting its “quality”.

Table 1 shows a classification of many known ion channels according to this criterion. Not surprisingly, potassium channels are the main representatives of slow restorative ion channels. By increasing the total outward current, their activation induces a negative feedback on membrane voltage variations that is responsible for neuron repolarization. On the other hand, physiologically described calcium channels are all slow regenerative. Their activation induces an increase of the total post-spike inward current, in contrast to potassium channels. This is the source, for instance, of afterdepolarization potentials (ADP). Interestingly, sodium channels can be either restorative, regenerative, or neutral according to their fast transient, resurgent, or persistent behavior, respectively.

It is important to observe that the restorative (resp. regenerative) nature of channels is not solely linked to the outward (resp. inward) nature of the current. For instance, transient sodium channels (although responsible for the regenerative spike upstroke) are slow restorative, because their slow variable inactivates an inward current, inducing a negative-feedback on membrane potential variations. Similarly, potassium channels can be slow regenerative when their slow inactivation massively decreases the outward current, like in the case of A-type potassium channels.

Although elementary, the classification above seems novel. It is motivated by the central message of this paper, that the balance between regenerative and restorative ion channels in slow timescale determines its neuronal excitability type. In the remainder of the paper, we simply write restorative (resp. regenerative) for slow restorative (resp. slow regenerative) channels.

Restorative and regenerative excitability in planar models

Planar models - that only consist of two state variables - have been instrumental to study excitability since the early days of neurodynamics [9, 10]. Empirical planar reductions of conductance based models only retain the (fast) voltage variable V and one slow gating variable n . Fast gating variables are set to steady-state (i.e. their fast variation is approximated as instantaneous), adaptation variables are treated as slowly varying parameters, and the slow gating variable n aggregates all slow variables, expressing each of them as a (curve-fitted) static function of n .

Motivated by the phase portrait of such an empirical reduction of the Hodgkin-Huxley model augmented with a calcium channel [11], our recent study [1] explores the neuronal excitability of the planar model

$$\dot{V} = V - \frac{V^3}{3} - n^2 + I_{app} \quad (1a)$$

$$\dot{n} = \varepsilon(n_\infty(V - V_0) + n_0 - n) \quad (1b)$$

whose phase portraits are reproduced in Fig. 1 for two distinct values of the parameter n_0 (an indirect representation of the calcium conductance in the high-dimensional model). The parameter $\varepsilon > 0$ characterizes the time-scale separation between V and n . The function $n_\infty(\cdot)$ has the standard sigmoid shape of conductance-based models and V_0 is the half-activation potential. The typical step responses of (1) are also reproduced in Fig. 1.

The spike generation mechanism in the phase portrait of Fig. 1 left is reminiscent of the of FitzHugh-Nagumo model and of the physiologically grounded planar reduction of Hodgkin-Huxley model by Rinzel [10]. It is associated to a reversible and sudden switch from rest to firing and has extensively been studied, with finer distinctions depending on the mathematical nature of the underlying bifurcation [12]. For further reading, see [13],[14, Section 7.1.3] and references therein.

The phase portrait in Fig. 1 right is in sharp contrast in that the electrophysiological response to a current input exhibits spike latency, plateau oscillations, and after depolarization potential (ADP). This specific signature, experimentally observed in many families of neurons, is fundamentally associated to the bistability illustrated in the phase portrait: namely, the robust coexistence of two stable attractors (a hyperpolarized resting potential and a limit cycle of periodic action potentials) and a saddle-separatrix that sharply separates their basins of attraction. The time evolution shown in the top figure is a consequence of this phase portrait and cannot be observed in FitzHugh-Nagumo like phase portraits. The distinction between the two phase portraits, the associated excitability types, and their relation with Hodgkin’s excitability classification [15] are further discussed in [1] and later in the paper.

A simple mathematical distinction between the two phase portraits shown in Fig. 1 is drawn from the Jacobian linearization of the model at the stable resting point (\bar{V}, \bar{n}) :

$$J = \left(\begin{array}{cc} \frac{\partial \dot{V}}{\partial V} & \frac{\partial \dot{V}}{\partial n} \\ \frac{\partial \dot{n}}{\partial V} & \frac{\partial \dot{n}}{\partial n} \end{array} \right) \bigg|_{(\bar{V}, \bar{n})} = \left(\begin{array}{cc} 1 - \bar{V}^2 & -2\bar{n} \\ \varepsilon \underbrace{\frac{\partial n_\infty}{\partial V} (\bar{V} - V_0)}_{>0} & -\varepsilon \end{array} \right).$$

The product of the partial derivatives $\frac{\partial \dot{V}}{\partial n} \frac{\partial \dot{n}}{\partial V} = -2\bar{n} \varepsilon \frac{\partial n_\infty}{\partial V} (\bar{V} - V_0)$ is negative on the left phase portrait ($\bar{n} > 0$), capturing the restorative nature of the gating variable, whereas it is positive on the right phase portrait ($\bar{n} < 0$), translating the regenerative nature of the gating variable. This difference is schematized in the block diagrams of Fig. 2. Accordingly, excitability in planar models is called restorative (resp. regenerative) when the gating variable provides negative (resp. positive) feedback close to the resting point:

Planar estorative excitability	Planar regenerative excitability
The model is said to be restorative at steady state if:	The model is said to be regenerative at steady state if:
$\left. \frac{\partial \dot{V}}{\partial n} \frac{\partial n_\infty}{\partial V} \right _{SS} < 0$	$\left. \frac{\partial \dot{V}}{\partial n} \frac{\partial n_\infty}{\partial V} \right _{SS} > 0$

The planar model (1) can smoothly switch from restorative to regenerative excitability, with a transition occurring for $\bar{n} = 0$, or, in algebraic terms,

$$\frac{\partial \dot{V}}{\partial n} \frac{\partial n_\infty}{\partial V} = 0 \tag{2}$$

A convenient way to algorithmically track this excitability switch is to use bifurcation analysis and to impose that the critical condition (2) coincides with a bifurcation of the model, which imposes the additional algebraic condition

$$\det J = -\varepsilon \left(\frac{\partial \dot{V}}{\partial V} + \frac{\partial \dot{V}}{\partial n} \frac{\partial n_\infty}{\partial V} \right) = 0. \tag{3}$$

Simultaneously imposing (2) and (3) implies

$$\frac{\partial \dot{V}}{\partial V} = 0, \tag{4}$$

which, in geometrical terms, corresponds to the transcritical bifurcation obtained for $I_{app} = \frac{2}{3}$ and illustrated in Fig. 3.

The theory of bifurcation unfolding is further exploited in [1] in order to classify all excitability types associated to the planar model in Fig. 1. This analysis results in five different types of excitability obtained by varying the two parameters (V_0, n_0) around the singular phase portrait of Fig. 3, center. The parameter n_0 acts in particular as the sole regulator of the balance between regenerative and restorative excitability by shifting the n -nullcline up and down: a positive n_0 corresponds to a phase portrait as in Fig. 3 left, whereas the phase portrait of Fig. 3 right is obtained for sufficiently negative n_0 . An early graphical manifestation of such phase portraits in conductance-based models is in [16, Figs. 17, 18, and 19]. Figure 4 delineates the two types of excitability in a two parameter chart. It contains the two types of excitability discussed above. The transition from restorative to regenerative excitability is always through a transcritical bifurcation. In addition, some paths traverse a small mixed region where a down regenerative steady state and an up restorative steady state coexist.

Our main contribution in the present paper is to show that the diagram in Fig. 4 is not an artifact of planar reduction but captures excitability transitions that can algorithmically be tracked in conductance-based models of arbitrary dimension by imposing a simple physiologically relevant algebraic condition.

Restorative and regenerative excitability in conductance based models

We start by grouping gating variables of a given conductance-based model according to their time scales. The family $\mathcal{G}_F = \{m_{Na,f}, m_{Na,p}, m_{K,A}, \dots\}$ collects fast gating variables. The gating variable $x^f \in [0, 1]$ denotes a generic member of this family. Similarly, the family $\mathcal{G}_S = \{h_{Na,f}, m_{K,DR}, m_{Ca,L}, \dots\}$ collects slow gating variables x^s , whereas $\mathcal{G}_A = \{h_{Ca,T}, h_{Na,R}, m_{K,M}, \dots\}$ collects adaptation variables x^a . For a given ion channel type i , the standard notation m_i (resp. h_i) is adopted for the activation (resp. inactivation) gating variable of the associated ionic current I_i . With these notations, a general neuron conductance-based model reads

$$C_m \dot{V} = - \sum_i \bar{g}_i m_i^{a_i} h_i^{b_i} (V - E_i) + I_{app}, \quad (5a)$$

$$\tau_{x^f}(V) \dot{x}^f = (x_\infty^f(V) - x^f), \quad (5b)$$

$$\tau_{x^s}(V) \dot{x}^s = (x_\infty^s(V) - x^s), \quad (5c)$$

$$\tau_{x^a}(V) \dot{x}^a = (x_\infty^a(V) - x^a), \quad (5d)$$

where the sum in (5a) is over all ion channels in the model, and (5b),(5c),(5d) hold for all the associated fast, slow, and adaptation variables, respectively. The activation (resp. inactivation) functions x_∞^f , x_∞^s are strictly monotone increasing (resp. decreasing) sigmoids. In the forthcoming analysis, all adaptation variables are treated as constant parameter, that is their slow evolution is neglected.

We will detect a switch from restorative to regenerative excitability by mimicking the two-dimensional algorithm of the previous section. We first impose the bifurcation condition $\det J = 0$, where J denotes the Jacobian of the subsystem (5a),(5b),(5c). The algebraic condition writes

$$\frac{\partial \dot{V}}{\partial V} + \sum_{x^f} \frac{\partial \dot{V}}{\partial x^f} \frac{\partial x_\infty^f}{\partial V} + \sum_{x^s} \frac{\partial \dot{V}}{\partial x^s} \frac{\partial x_\infty^s}{\partial V} = 0, \quad (6)$$

where the sums are over all fast and slow variables, respectively. The particular form of equation (6) is a direct consequence of the specific structure of conductance-based models, that is, parallel interconnection of two-dimensional feedback loops involving the voltage dynamics (5a) and one of the gating variable dynamics (5b),(5c).

As for the planar model (1), we track the switch between restorative and regenerative excitability by imposing the high-dimensional equivalent of the balance condition (2). We therefore look for solutions of (6) satisfying the ansatz

$$\sum_{x^s} \frac{\partial \dot{V}}{\partial x^s} \frac{\partial x_\infty^s}{\partial V} = 0. \quad (7)$$

The two conditions (6),(7) now imply

$$\det J_f = 0, \quad (8)$$

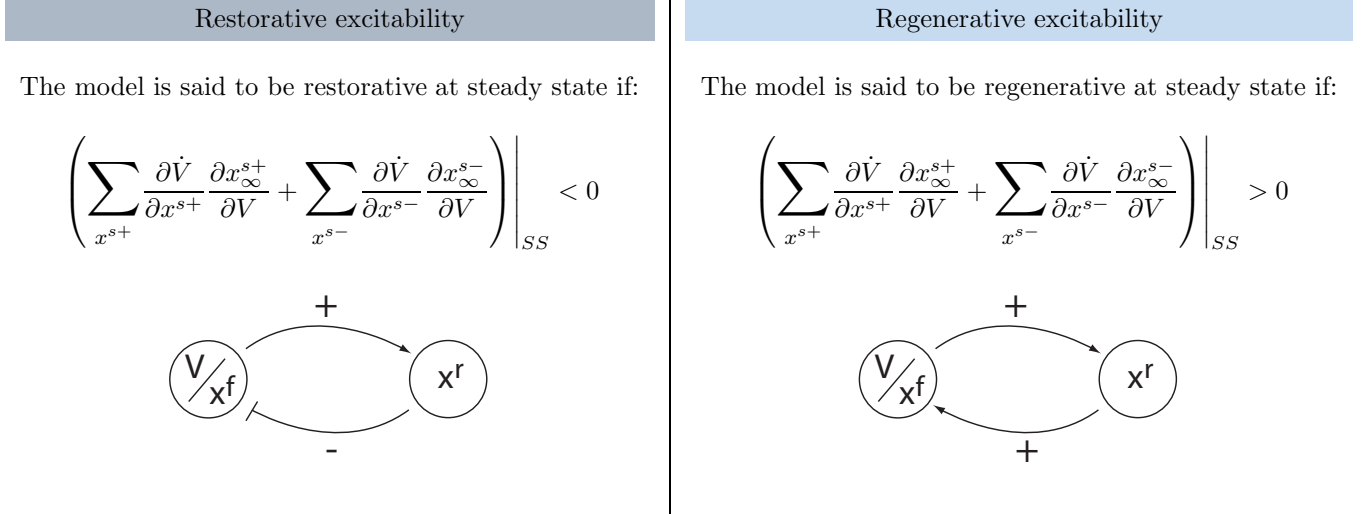
where J_f denotes the Jacobian of the fast subsystem (5a),(5b). We show in Supplementary Material S1 that the corresponding bifurcation is necessarily transcritical [17, Section 3.2].

The singularity condition (8) is the high-dimensional counterpart of the V -nullcline self-intersection in the planar model. It reflects the geometric nature of the transcritical bifurcation, that is, a robust geometrical object that exists independently of the timescale separation and persists in the singular limit of an infinite timescale separation, regardless of the system dimension. Our ansatz makes the proposed analysis completely robust against the model time constants. The time constants are only used to classify the gating variables in the three physiological groups.

We split \mathcal{G}_S in the two subfamilies \mathcal{G}_{S^+} , which contains *regenerative* slow gating variables x^{s^+} , and \mathcal{G}_{S^-} , which contains *restorative* slow gating variables x^{s^-} . The balance condition (7) is then rewritten as

$$\underbrace{\sum_{x^{s^+}} \overbrace{\left. \frac{\partial \dot{V}}{\partial x^{s^+}} \frac{\partial x_\infty^{s^+}}{\partial V} \right|_{TC}}^{> 0}}_{\text{regenerative gates}} + \underbrace{\sum_{x^{s^-}} \overbrace{\left. \frac{\partial \dot{V}}{\partial x^{s^-}} \frac{\partial x_\infty^{s^-}}{\partial V} \right|_{TC}}^{< 0}}_{\text{restorative gates}} = 0 \quad (9)$$

to express a balance between restorative and regenerative ion channels. It is the high-dimensional counterpart of (2) and it provides a rigorous high-dimensional generalization of restorative and regenerative excitability:



The insight provided by the planar model of the previous section predicts that the switch of excitability detected by the balance equation (9) will lead to the accompanying distinct electrophysiological signatures of Fig. 1.

Tracking excitability switches in the squid giant axon

The Hodgkin-Huxley (HH) model [2] provides a non-physiological, but historical and experimentally verified tutorial for tracking a switch of excitability in conductance based models. The model reads

$$C\dot{V} = -\bar{g}_K n^4 (V - V_K) - \bar{g}_{Na} m^3 h (V - V_{Na}) - g_l (V - V_l) + I_{app}, \quad (10a)$$

$$\tau_m(V) \dot{m} = (m_{\infty}(V) - m), \quad (10b)$$

$$\tau_h(V) \dot{h} = (h_{\infty}(V) - h), \quad (10c)$$

$$\tau_n(V) \dot{n} = (n_{\infty}(V) - n), \quad (10d)$$

where m is the fast sodium channel activation while the sodium channel inactivation h and the potassium channel activation n are the slow gating variables. We set all time constants to one, because this simplification has no effects on the algebraic conditions (7) and (8). The Jacobian of (10) reads

$$J = \begin{bmatrix} \frac{\partial \dot{V}}{\partial V} & \frac{\partial \dot{V}}{\partial m} & \frac{\partial \dot{V}}{\partial h} & \frac{\partial \dot{V}}{\partial n} \\ \frac{\partial m_{\infty}}{\partial V} & -1 & 0 & 0 \\ \frac{\partial h_{\infty}}{\partial V} & 0 & -1 & 0 \\ \frac{\partial n_{\infty}}{\partial V} & 0 & 0 & -1 \end{bmatrix}. \quad (11)$$

The upper-left block is the Jacobian of the fast (V, m) subsystem. Imposing the singularity condition (8) yields

$$\frac{\partial \dot{V}}{\partial V} \Big|_{TC} + \frac{\partial \dot{V}}{\partial m} \frac{\partial m_{\infty}}{\partial V} \Big|_{TC} = 0, \quad (12a)$$

while the balance equation (9) reads

$$\frac{\partial \dot{V}}{\partial n} \frac{\partial n_{\infty}}{\partial V} \Big|_{TC} + \frac{\partial \dot{V}}{\partial h} \frac{\partial h_{\infty}}{\partial V} \Big|_{TC} = 0 \quad (13a)$$

Note that (12) and (13) imply the bifurcation condition $\det J = 0$ in (11).

At first sight, the balance condition (13) cannot be satisfied because both sodium and potassium channels are restorative channels according to their corresponding kinetics in the model, and in agreement with our proposed classification. This is consistent with the fact that the excitability of the HH model is always restorative in physiological conditions.

However, it was long recognized [18] that potassium channels can generate an inward current at steady-state if the extracellular K^+ concentration is sufficiently large. Indeed, any change in extracellular potassium concentration induces a change in the potassium reversal potential, as expressed by the Nernst equation. This suggests to use the potassium reversal potential V_K as a bifurcation parameter in HH model in order to satisfy the balance equation

$$\underbrace{\left. \frac{\partial \dot{V}}{\partial n} \frac{\partial n_\infty}{\partial V} \right|_{TC}}_{n: \text{ regenerative gating}} \overset{! > 0}{=} + \underbrace{\left. \frac{\partial \dot{V}}{\partial h} \frac{\partial h_\infty}{\partial V} \right|_{TC}}_{h: \text{ restorative gating}} \overset{< 0}{=} = 0 \quad (14)$$

where potassium now acts as a regenerative gating variable provided that $V_K > V_{SS}$. Physiologically, condition (14) imposes that the potassium Nernst potential is large enough for the regenerativity of the potassium activation to balance the restorative effects of the sodium current inactivation.

The two conditions (12) and (14) can numerically be solved to determine the critical values V_K^c and V^c . The value of the applied current at the transcritical bifurcation is then determined from (10a), which gives

$$I_{app}^c = \bar{g}_K n_\infty^4(V^c)(V^c - V_K^c) + \bar{g}_{Na} m_\infty^3(V^c) h_\infty(V^c)(V^c - V_{Na}) + g_l(V^c - V_l).$$

The numerical bifurcation diagram in Fig. 5A confirms the transcritical bifurcation at V_K^c . That bifurcation diagram is drawn by varying V_K together with applied current I_{app} , following the affine reparametrization described in Supplementary Material S1. More precisely,

$$I_{app}(V_K) = I_{app}^c - \bar{g}_K n_\infty^4(V^c)(V_K - V_K^c).$$

Mathematically, this reparametrization imposes one of the defining conditions of the transcritical bifurcation. Physiologically, its effect is to keep the net current constant at steady-state V^c (*i.e.* $I_{ion}(V_K) + I_{app}(V_K) = 0$): as V_K is varied, the observed switch in the excitability type does not rely on changes in the net current across the membrane, but solely on changes in its dynamical properties.

The bifurcation diagram in Fig. 5A provides informations on the model excitability also far from the transcritical values. For highly hyperpolarized V_K , the model is purely restorative and exhibits the typical excitable behavior of the original Hodgkin-Huxley model [1, Figure 8]. As V_K is increased, a stable regenerative steady-state is born in a saddle-node bifurcation. At this transition, the system switches to a mixed excitability type. Short current pulses let the system switch between the depolarized restorative steady state and the hyperpolarized regenerative stable steady state (Fig. 5B,middle). The associated bifurcation diagram and phase portrait are reproduced in Fig. 5C,D,middle. Finally, further increase of V_K let the restorative steady state exchanges its stability with a (regenerative) saddle at the transcritical bifurcation (and, soon after, lose stability in a Hopf bifurcation) and the system switches to regenerative excitability. The regenerative steady state coexists in this case with the spiking limit cycle attractor. Current pulses switch the systems between the two attractors (Fig. 5B,right). The associated bifurcation diagram and phase portrait are reproduced in Fig. 5C,D,right.

The same qualitative excitability switch was described by Rinzel in [10], who linked the appearance of a bistable behavior to the inward nature of potassium current at steady-state for sufficiently depolarized V_K . *In vitro* recordings of the squid giant axon with isotonic extracellular K^+ concentration show the same transition [18].

Tracking excitability switches in conductance-based models

The mathematical analysis of the previous sections follows an algorithm that allows to detect a transcritical bifurcation in generic conductance based models of arbitrary dimension and to track associated excitability

switches. The steps of the algorithm are summarized in Table 2. For simplicity and conciseness, we restrict our attention to the modulation of only one regenerative ionic current at a time. However, a similar algorithm can be written for an arbitrary modulation of ionic currents (by variation of maximal conductance(s), adaptation variable(s), or reverse potential(s)) that brings the model to the balance expressed in (9).

We now apply this algorithm to a number of published conductance-based models and show that all these models can switch between restorative and regenerative excitability through a transcritical bifurcation, as sketched in Fig. 6. Figure 6 indicates two qualitatively distinct paths from restorative to regenerative excitability: one path traversing the mixed excitability region just described with Hodgkin-Huxley model (Fig. 5A) and one path switching directly from restorative to regenerative excitability through the TC bifurcation that will be illustrated on the dopaminergic neuron model.

Dopaminergic (DA) neuron model

Model equations and parameters are taken from [3]. This is the model that originally motivated [11].

(i) **Classification of gating variables as fast (\mathcal{G}_F), slow (\mathcal{G}_S), and adaptation (\mathcal{G}_A) variables**

The model includes fast sodium channels ($I_{Na,f}$), delayed-rectifier potassium channels ($I_{K,DR}$), L-type calcium channels ($I_{Ca,L}$), small conductance calcium-activated potassium (SK) channels ($I_{K,Ca}$), and calcium pumps ($I_{Ca,pump}$). We classify model variables as follows

- $\mathcal{G}_F = \{m_{Na,f}\}$
- $\mathcal{G}_{S,-} = \{h_{Na,f}, m_{K,DR}\}$ and $\mathcal{G}_{S,+} = \{m_{Ca,L}\}$
- $\mathcal{G}_A = \{[Ca^{2+}]_{in}\}$

In order to unfold excitability switches, SK channel density is set to zero, since SK channels drastically attenuate DA neuron excitability by activating a strong calcium regulated potassium current [19, 20, 21]. The intracellular calcium concentration is fixed at $[Ca^{2+}]_{in} = 300 \text{ nM}$.

(ii) **Balance equation and choice of the bifurcation parameter**

The only source of regenerative excitability is provided by L-type calcium channels. The balance equation reads

$$\left. \frac{\partial \dot{V}}{\partial m_{Ca,L}} \frac{\partial m_{Ca,L,\infty}}{\partial V} \right|_{TC} = - \left(\left. \frac{\partial \dot{V}}{\partial h_{Na,f}} \frac{\partial h_{Na,f,\infty}}{\partial V} + \frac{\partial \dot{V}}{\partial m_{K,DR}} \frac{\partial m_{K,DR,\infty}}{\partial V} \right) \right|_{TC}. \quad (15)$$

We use the L-type calcium channel density $\bar{g}_{Ca,L}$ as the bifurcation parameter (*i.e.* $\lambda = \bar{g}_{Ca,L}$).

Solving Steps (iii) and (iv) of the algorithm above gives the following results (in this and the subsequent tables, the reported critical values are not exact, but rounded to the last significant digit):

V^c	$\bar{g}_{Ca,L}^c$	I^c
-64.9167 mV	1.9473 mS/cm ²	9.5436 μ A/cm ²

The critical value $\bar{g}_{Ca,L}^c$ is roughly 1.5 times smaller than the nominal parameter value in [3], which is consistent with the observation that the original model exhibits regenerative excitability during SK channel blockade.

The resulting bifurcation diagram is drawn in Fig. 7A. In addition to confirming the existence of a transcritical bifurcation for the computed values, it reveals the excitability switches induced by changes in L-type calcium channel density in this model: in the absence of L-type calcium channels, the model exhibits restorative excitability. As $\bar{g}_{Ca,L}$ increases, a saddle point and an unstable node emerge at a saddle-node bifurcation, which induces no excitability switch. Further increase of $\bar{g}_{Ca,L}$ causes a transcritical bifurcation, where the stable point and the saddle exchange their stability. At this point, the stable steady-state becomes regenerative, and the model switches to regenerative excitability.

These excitability switches induce the predicted changes in the electrophysiological signatures, as illustrated in Fig. 7B. Whereas the DA neuron model instantaneously reacts to a step input of depolarizing current for

$\bar{g}_{Ca,L} < \bar{g}_{Ca,L}^c$, it exhibits electrophysiological signature of regenerative excitability such as spike latency, plateau oscillations and ADP as soon as $\bar{g}_{Ca,L}$ becomes higher than $\bar{g}_{Ca,L}^c$. In addition, the model becomes strongly bistable.

Thalamic relay (RE) neuron model

Model equations and parameters are taken from [4].

(i) **Classification of gating variables as fast (\mathcal{G}_F), slow (\mathcal{G}_S), and adaptation (\mathcal{G}_A) variables**

The model includes fast sodium channels $I_{Na,f}$, delayed-rectifier potassium channels $I_{K,DR}$ and T-type calcium channels $I_{Ca,T}$. We classify model variables as follows

- $\mathcal{G}_F = \{m_{Na,f}\}$
- $\mathcal{G}_{S,-} = \{h_{Na,f}, m_{K,DR}\}$ and $\mathcal{G}_{S,+} = \{m_{Ca,T}\}$
- $\mathcal{G}_A = \{h_{Ca,T}\}$

(ii) **Balance equation and choice of the bifurcation parameter**

The only source of regenerative excitability is provided by T-type calcium channels. The associated balance equation reads

$$\left. \frac{\partial \dot{V}}{\partial m_{Ca,T}} \frac{\partial m_{Ca,T,\infty}}{\partial V} \right|_{TC} = - \left(\left. \frac{\partial \dot{V}}{\partial h_{Na,f}} \frac{\partial h_{Na,f,\infty}}{\partial V} + \frac{\partial \dot{V}}{\partial m_{K,DR}} \frac{\partial m_{K,DR,\infty}}{\partial V} \right) \right|_{TC}.$$

T-type calcium channels are dynamically regulated by a (slow) voltage-gated inactivation $h_{Ca,T}$. We use this variable as the bifurcation parameter (*i.e.* $\lambda = h_{Ca,T}$).

Solving Steps (iii) and (iv) of the algorithm above gives the following results:

V^c	$\bar{h}_{Ca,T}^c$	I^c
-61.5561 mV	0.0041	0.9074 nA/cm ²

Since $\bar{h}_{Ca,T}^c \in (0, 1)$, the model dynamically switches between restorative and regenerative excitability when $h_{Ca,T}$ crosses the critical value, and the electrophysiological signatures are consistent with the excitability switches. See Fig. 8.

Thalamic reticular (RT) neuron model

Model equations and parameters are taken from [5], maximal conductances are adapted as in [11].

(i) **Classification of gating variables as fast (\mathcal{G}_F), slow (\mathcal{G}_S), and adaptation (\mathcal{G}_A) variables**

The model includes fast sodium channels $I_{Na,f}$, delayed-rectifier potassium channels $I_{K,DR}$ and T-type calcium channels $I_{Ca,T}$. We classify model variables as follows

- $\mathcal{G}_F = \{m_{Na,f}\}$
- $\mathcal{G}_{S,-} = \{h_{Na,f}, m_{K,DR}\}$ and $\mathcal{G}_{S,+} = \{m_{Ca,T}\}$
- $\mathcal{G}_A = \{h_{Ca,T}\}$

(ii) **Balance equation and choice of the bifurcation parameter**

The only source of regenerative excitability is provided T-type calcium channels. The associated balance equation has the same structure as for the thalamic relay neuron model considered above. Along the same line, we choose the T-type calcium channel inactivation $h_{Ca,T}$ as the bifurcation parameter (*i.e.* $\lambda = h_T$).

Solving Steps (iii) and (iv) of the algorithm above gives the following results:

V^c	$\bar{h}_{Ca,T}^c$	I^c
-48.8063 mV	0.1780	-0.82484 nA

As in the case of the thalamic relay neuron model, the T-type calcium channel inactivation generates a dynamical switch between restorative and regenerative excitability, significantly affecting neuron response to external inputs (Fig. 8).

Aplysia R15 neuron model

Model equations and parameters are taken from [6].

(i) **Classification of gating variables as fast (\mathcal{G}_F), slow (\mathcal{G}_S), and adaptation (\mathcal{G}_A) variables**

The model includes fast sodium channels $I_{Na,f}$, delayed-rectifier potassium channels $I_{K,DR}$, slow L-type calcium channels $I_{Ca,L}$ and calcium-activated potassium channels $I_{K,Ca}$. We classify model variables as follows

- $\mathcal{G}_F = \{m_{Na,f}\}$
- $\mathcal{G}_{S,-} = \{h_{Na,f}, m_{K,DR}\}$ and $\mathcal{G}_{S,+} = \{m_{Ca,L}\}$
- $\mathcal{G}_A = \{[Ca^{2+}]_{in}\}$

The intracellular calcium conductance is fixed at $[Ca^{2+}]_{in} = 0.09nM$.

(ii) **Balance equation and choice of the bifurcation parameter**

As in the case of DA neurons, the source of regenerative excitability is provided by L-type calcium channels, and we take their maximal conductance $\bar{g}_{Ca,L}$ as the bifurcation parameter. The associated balance equation has the same structure as for the DA neuron model considered above.

Solving Steps (iii) and (iv) of the algorithm above gives the following results:

V^c	$\bar{g}_{Ca,L}^c$	I^c
-48.0516 mV	$5.4054 \cdot 10^{-5}$ mS/cm ²	-0.0318 $\mu A/cm^2$

Comparing the critical value $\bar{g}_{Ca,L}^c$ with the original value $\bar{g}_{Ca,L} = 4 \cdot 10^{-3}$ mS/cm² shows that the bursting model proposed in [6] exhibits strong regenerative excitability. Switches of electrophysiological signatures are illustrated in Fig. 8.

Cerebellar granular cell (GC) model

Model equations and parameters are taken from [7].

(i) **Classification of gating variables as fast (\mathcal{G}_F), slow (\mathcal{G}_S), and adaptation (\mathcal{G}_A) variables**

The model includes the following ion channels: fast ($I_{Na,f}$), persistent ($I_{Na,P}$) and resurgent sodium channels ($I_{Na,R}$); N-type calcium channels ($I_{Ca,N}$); delayed rectifier ($I_{K,DR}$), A-type ($I_{K,A}$), inward rectifier ($I_{K,IR}$), calcium activated ($I_{K,Ca}$) and slow potassium channels ($I_{K,slow}$). We classify model variables as follows

- $\mathcal{G}_F = \{m_{Na,f}, m_{Na,P}\}$
- $\mathcal{G}_{S,-} = \{h_{Na,f}, m_{K,DR}, m_{K,A}, m_{K,IR}\}$ and $\mathcal{G}_{S,+} = \{m_{Na,R}, m_{Ca,N}\}$
- $\mathcal{G}_A = \{h_{Na,R}, h_{Ca,N}, h_{K,A}, m_{K,slow}\}$

We set the persistent and calcium-activated currents to zero (these two channels do not impact excitability type as anticipated by our classification and shown by D'Angelo and colleagues [7]). The inactivation of the A-type potassium current is fixed at $h_{K,A} = 0.02$ and the activation of the slow potassium current is fixed at $m_{K,slow} = 0.13$.

(ii) **Balance equation and choice of the bifurcation parameter**

The neuron model possesses two sources of regenerative excitability: resurgent sodium channels and N-type calcium channels. As in the case of T-type calcium channels mentioned above, these two channels possess an inactivation gate, which is used as the bifurcation parameter. We apply our algorithm by varying the parameter of one regenerative current while fixing the other at different values. This permits to draw an approximated hypersurface in the $(h_{Ca,N}, h_{Na,R})$ plane at which the balance equation is satisfied and the model undergoes the transcritical bifurcation and the associated excitability switch. The two balance equations read, respectively:

$$\left. \frac{\partial \dot{V}}{\partial m_{Na,R}} \frac{\partial m_{Na,R,\infty}}{\partial V} \right|_{TC} = - \left(\frac{\partial \dot{V}}{\partial h_{Na,f}} \frac{\partial h_{Na,f,\infty}}{\partial V} + \sum_{y=DR, A, IR} \frac{\partial \dot{V}}{\partial m_{K,y}} \frac{\partial m_{K,y,\infty}}{\partial V} + \frac{\partial \dot{V}}{\partial m_{Ca,N}} \frac{\partial m_{Ca,N,\infty}}{\partial V} \right) \Bigg|_{TC},$$

$$\left. \frac{\partial \dot{V}}{\partial m_{Ca,N}} \frac{\partial m_{Ca,N,\infty}}{\partial V} \right|_{TC} = - \left(\frac{\partial \dot{V}}{\partial h_{Na,f}} \frac{\partial h_{Na,f,\infty}}{\partial V} + \sum_{y=DR, A, IR} \frac{\partial \dot{V}}{\partial m_{K,y}} \frac{\partial m_{K,y,\infty}}{\partial V} + \frac{\partial \dot{V}}{\partial m_{Na,R}} \frac{\partial m_{Na,R,\infty}}{\partial V} \right) \Bigg|_{TC},$$

Solving Steps (iii) and (iv) of the algorithm one obtains the parameter chart in Fig. 9. These results show that both channels can induce a dynamical switch in excitability. However, the N-type calcium channel contributes much more to regenerative excitability than the resurgent sodium channel in this model: as soon as $h_{Ca,N} \gtrsim 0.03$ the model is in regenerative excitability for all values of $h_{Na,R}$. On the contrary, when $h_{Ca,N} = 0$ the inactivation of resurgent sodium channel should be more than a half de-inactivated for the model to exhibit regenerative excitability.

The balance equation determines a switch from restorative to regenerative excitability

As illustrated in Figure 4, the significance of the transcritical bifurcation is that it delineates in the parameter space the boundary of a specific type of excitability and that this boundary is determined by a simple physiological balance (Eq. 9) between restorative and regenerative channels.

Specific to regenerative excitability is the bistable (right) phase portrait of Figure 1. For the five analyzed conductance-based models, our bifurcation analysis of the full model confirms the existence of a bistable range beyond the transcritical bifurcation, where a regenerative resting state and a spiking limit cycle coexist. In each case, the bistability range is obtained for the nominal time scales of the published model and is robust to a variation of time scales. In each case, the bistability range is also neuromodulated, that is, determined by conductance parameters that are known to vary in slower time scales and/or across neurons of a same type.

It is important to distinguish this robust and physiologically regulated bistability from other types of bistability that can be encountered in conductance-based models. Figure 10 qualitatively illustrates three typical bistable phase portraits associated to the planar model (1) that exhibit the coexistence of a stable resting state and of a spiking limit cycle. The first two are associated to restorative excitability and are extensively studied in the literature. See, e.g., [13, 14] and references therein. Only the third one is associated to regenerative excitability.

The three bistable phase portraits share the common feature of “hard excitation”: as the amplitude of a step input depolarizing current is increased, the response of the neuron abruptly switches from no oscillation to high frequency spiking. Following the historical classification of Hodgkin [15], the three situations correspond to Class II neurons, as opposed to Class I neurons for which the spiking frequency gradually increases with the depolarizing current amplitude.

Hard excitation can be a manifestation either of a switch-like monostable bifurcation diagram or of a hysteretic bistable bifurcation diagram. By definition, the three bistable phase portraits in Figure 10 give rise to hysteretic bifurcation diagrams. But for the two bistable phase portraits associated to restorative excitability, the hysteresis is highly dependent on the time scale separation, *i.e.*, the ratio ε between the fast and slow time constants. In the case of the first phase portrait (subcritical Hopf bifurcation), asymptotic analysis shows that the hysteresis vanishes as $\mathcal{O}(e^{-1/\varepsilon})$. In the case of second phase portrait (saddle-homoclinic bifurcation), the situation is even worse because for small $\varepsilon > 0$ the system necessarily undergoes a monostable saddle-node on invariant circle bifurcation. In fact, the second phase portrait is not physiological for conductance based-models.

For instance, in the hypothetical $I_{Na,p} + I_K$ conductance-based model considered in [14, Fig. 6.44], the time constant of the potassium activation must be set to below $0.17ms$ to create a saddle-homoclinic bifurcation, which is roughly 40 times smaller than its physiological value and even smaller than the fast time constant. A geometric proof of the generality of this fact is provided in [1]. The conclusion is that hysteresis associated to restorative excitability is at best very small (if any) in physiologically plausible conductance based models, which makes their electrophysiological signatures similar to those associated to a switch-like monostable bifurcation diagram.

In sharp contrast, the hysteresis associated to regenerative excitability is barely affected by the time-scale separation. Instead it is regulated by conductance parameters whose modulation is physiological (for instance, a regenerative ion channel density). The extended hysteresis is what determines the specific electrophysiological signature of regenerative excitability: a pronounced spike latency, a possible plateau oscillation, and an after depolarization potential. As a consequence, those features cannot be robustly reproduced in physiologically plausible conductance based models of restorative excitability. Because those features are important markers of modern electrophysiology [22, 23], the distinction between restorative and regenerative excitability seems physiologically relevant, beyond the possible shared feature of hard excitation.

In conclusion, the bistability associated to regenerative excitability is specific in that it produces a robust electrophysiological signature in physiologically plausible parameter ranges and consistent with many experimental observations. It is in that sense that balance equation delineates a switch of excitability of physiological relevance.

A refined classification of neuronal excitability

Early in the history of neurodynamics [15], Hodgkin proposed a classification of excitability in three different classes:

Class I: The spiking frequency vs. input current amplitude (f/I) curve is continuous, *i.e.*, the spiking frequency continuously increases from zero to high-frequency firing as the input current amplitude rises. Class I excitability is also referred to as “soft” excitation.

Class II: The f/I is discontinuous, *i.e.*, the spiking frequency abruptly switches from zero to high-frequency firing as the amplitude of the applied current is raised above a certain threshold. Class II excitability is also referred to as “hard” excitation.

Class III: The spiking frequency is zero for all amplitudes of the applied current. Transient action potentials can be generated in response to high-frequency stimuli.

Because regenerative excitability exhibits hard excitation, it is a physiologically distinct subtype of Class II excitability.

Bifurcation theory helps relating this physiological classification to mathematical signatures of the associated neuron models. Distinct bifurcations delineate the different excitability classes as well as the different excitability mechanisms within a given class. They are summarized in Fig. 11.

Ermentrout [12] showed that Class I excitability arises from a saddle-node on invariant circle bifurcation, whereas Class II excitability arises from a Hopf bifurcation. Both bifurcations correspond to examples of restorative excitability in the terminology of the present paper and the transition between Class I and II is governed by a Bogdanov-Takens bifurcation.

Our recent paper [1] further expands this classification to account for regenerative excitability. Regenerative excitability (called Type IV in [1]) arises from a (singularly perturbed) saddle-homoclinic bifurcation and the transition from restorative to regenerative excitability always involves a transcritical bifurcation.

Discussion

A simple and robust balance equation identifies a transcritical bifurcation in arbitrary conductance based models

Motivated by a geometric analysis of a qualitative phase portrait, we have proposed an algorithm that easily detects a transcritical bifurcation in arbitrary conductance based models. Owing to the special structure of such models, the algorithm leads to solving an algebraic equation of remarkable simplicity and physiological relevance: a balance between slow restorative and slow regenerative ion channels. The condition is also robust because the balance is independent of the detailed kinetics, even though it critically relies on a classification of variables in three well separated time-scales, in good agreement with what is known on ion channels kinetics [8].

The ubiquity of a transcritical bifurcation in conductance-based models

The detection of the transcritical bifurcation relies on the sole existence of a physiological balance between restorative and regenerative ion channels. Given that all neuronal models possess restorative sodium and potassium channels, this implies that a transcritical bifurcation exists in every conductance-based model that possesses at least one regenerative ion channel. Moreover, the channel balance, and therefore the TC bifurcation, are readily detectable in a model of arbitrary dimension (both in the state and parameters): the balance (9) simply defines a hypersurface in the parameter space that can algebraically be tracked under arbitrary parameter variations, as illustrated with in the GC model above.

In spite of its ubiquity and of its physiological significance, we are not aware of an earlier reference to a transcritical bifurcation in conductance based models. A reason for this omission might be accidental: there are no regenerative channels in the seminal model of Hodgkin and Huxley (unless one modifies the potassium resting potential V_k) and this model has been the inspiration of most mathematical analyses of conductance-based models.

For the same reason, it seems physiologically relevant to distinguish between restorative and regenerative excitability beyond Hodgkin’s classification of Class I (“soft”) and Class II (“hard”) excitability. Regenerative (and restorative) excitability faithfully capture the presence (or the absence) of specific electrophysiological signatures of modern electrophysiology such as spike latency, afterdepolarization potentials, or robust coexistence of resting state and repetitive spikes.

A single mathematical prediction applies to many distinct physiological observations

Although purely mathematical in nature, the transcritical bifurcation has a remarkable predictive value in several published conductance based models. In each of the six analysed models, the proposed algorithm identifies a physiological parameter that acts as a tuner of neuronal excitability in a physiologically plausible range and in full agreement with existing experimental data. At the same time, the distinct nature of the regulating parameter, which can be either the maximal conductance or the inactivation gating variable of a regenerative ion channel depending on the neuron model, is associated to distinctly different regulation mechanisms.

Reduced modelling should retain the balancing channel

The classification of gating variables in three distinct time scales is an essential modelling step both for the proposed algorithm and for the reduction of full conductance-based models to low-dimensional models that can be used in population studies [24]. Despite the inherent robustness of time-scale separation analysis, this classification is a limitation of the proposed approach if the model contains ion channels with poorly known kinetics. When all slow ion channels are properly identified, they can be aggregated in a single slow variable to lead to a second order model of the type (1), where the single parameter n_0 captures the restorative or regenerative nature of the aggregated slow variable. Further reduction to a one-dimensional hybrid model with reset is possible thanks to the time-scale separation between the voltage V and the slow variable n . This reduction is illustrated in [11] on the thalamic TC neuron and the reduced model remarkably retains the switch of excitability of its high-dimensional counterpart. In contrast, a reduced model will lose the switch of excitability of the full conductance-based model when a regenerative ion channel is treated as a fast gating variable. It is

for instance common in model reduction to set the activation a calcium channel to steady state. This amounts to treat the calcium activation as a fast variable, which makes the channel “slow restorative” in the terminology of this paper. If the calcium channel is the only source of regenerative excitability, then the reduced model will not retain features of regenerative excitability.

Neuronal excitability is regulated

In each of the analysed conductance-based models, the balance equation responsible for the switch of excitability is satisfied for a set of parameters that is close to the published parameter values. This observation supports the hypothesis that neuronal excitability is tightly regulated by molecular mechanisms and that the influence of the channel balance condition on neuronal excitability might play a role in neuronal signaling.

Materials and Methods

Numerical analysis

Numerical temporal traces of the different neurons (Figs. 1, 5, 7, 8) were reproduced by implementing in MATLAB (available at <http://www.mathworks.com>) the original models as described in the associated papers. The phase portraits in Figures 1 and 3 were hand-drawn using the Open Source vector graphics editor Inkscape (<http://inkscape.org>). The phase portraits in Figure 5 were numerically drawn with MATLAB by implementing the planar model in [10] and subsequently modified with Inkscape. The bifurcation diagrams in Figures 5, 6, and 7 were drawn by implementing the algorithm of Table 2 in MATLAB. No figure or part of figure was reproduced from other published works.

Acknowledgment

The reviewers are gratefully acknowledged for insightful comments and suggestions about the original version of the manuscript.

References

- [1] Franci A, Drion G, Sepulchre R (2012) An organizing center in a planar model of neuronal excitability. *SIAM J Appl Dyn Syst* 11: 1698-1722.
- [2] Hodgkin A, Huxley A (1952) A quantitative description of membrane current and its application to conduction and excitation in nerve. *J Physiol* 117: 500-544.
- [3] Drion G, Massotte L, Sepulchre R, Seutin V (2011) How modeling can reconcile apparently discrepant experimental results: The case of pacemaking in dopaminergic neurons. *PLoS Comput Biol* 7: e1002050.
- [4] Destexhe A, Neubig M, Ulrich D, Huguenard J (1998) Dendritic low-threshold calcium currents in thalamic relay cells. *J Neurosci* 18: 3574-3588.
- [5] Destexhe A, Contreras D, Steriade M, Sejnowski T, Huguenard J (1996) In vivo, in vitro, and computational analysis of dendritic calcium currents in thalamic reticular neurons. *J Neurosci* 16: 169-185.
- [6] Rinzel J, Lee Y (1987) Dissection of a model for neuronal parabolic bursting. *J Math Biol* 25: 653-675.
- [7] D’Angelo E, Nieus T, Maffei A, Armano S, Rossi P, et al. (2001) Theta-frequency bursting and resonance in cerebellar granule cells: experimental evidence and modeling of a slow K⁺-dependent mechanism. *J Neurosci* 21: 759-770.
- [8] Hille B (1984) *Ionic channels of excitable membranes*. Sunderland, MA: Sinauer Associates Inc, 426 pp.
- [9] FitzHugh R (1961) Impulses and physiological states in theoretical models of nerve membrane. *Biophysical J* 1: 445-466.

- [10] Rinzel J (1985) Excitation dynamics: insights from simplified membrane models. In: Federation proceedings. Fed Proc, volume 44, p. 2944.
- [11] Drion G, Franci A, Seutin V, Sepulchre R (2012) A novel phase portrait for neuronal excitability. PLoS ONE 7: e41806.
- [12] Ermentrout GB (1996) Type I membranes, phase resetting curves, and synchrony. Neural Comput 8: 979-1001.
- [13] Rinzel J, Ermentrout G (1989) Analysis of neural excitability and oscillations. In: Methods in neuronal modeling. MIT Press, pp. 135–169.
- [14] Izhikevich E (2007) Dynamical Systems in Neuroscience: The Geometry of Excitability and Bursting. MIT Press.
- [15] Hodgkin A (1948) The local electric changes associated with repetitive action in a non-medullated axon. J Physiol 107: 165–181.
- [16] Rubin JE, Terman D (2004) High frequency stimulation of the subthalamic nucleus eliminates pathological thalamic rhythmicity in a computational model. J Comput Neurosci 16: 211-235.
- [17] Strogatz S (2001) Nonlinear dynamics and chaos: with applications to physics, biology, chemistry, and engineering. Westview Press.
- [18] Moore J (1959) Excitation of the squid axon membrane in isosmotic potassium chloride. Nature 183: 265-266.
- [19] Waroux O, Massotte L, Alleva L, Graulich A, Thomas E, et al. (2005) SK channels control the firing pattern of midbrain dopaminergic neurons in vivo. Eur J Neurosci 22: 3111–3121.
- [20] Drion G, Seutin V, Sepulchre R (2012) Mitochondrion-and endoplasmic reticulum-induced SK channel dysregulation as a potential origin of the selective neurodegeneration in Parkinsons disease. Systems Biology of Parkinson’s Disease : 57–79.
- [21] Ji H, Hougaard C, Herrik K, Strøbæk D, Christophersen P, et al. (2009) Tuning the excitability of midbrain dopamine neurons by modulating the Ca²⁺ sensitivity of SK channels. Eur J Neurosci 29: 1883–1895.
- [22] Fuentealba P, Timofeev I, Bazhenov M, Sejnowski TJ, Steriade M (2005) Membrane bistability in thalamic reticular neurons during spindle oscillations. J Neurophys 93: 294-304.
- [23] Junek S, Kludt E, Wolf F, Schild D (2010) Olfactory coding with patterns of response latencies. Neuron 67: 872 - 884.
- [24] Izhikevich E, Edelman G (2008) Large-scale model of mammalian thalamocortical systems. Proc Natl Acad Sci U S A 105: 3593-3598.

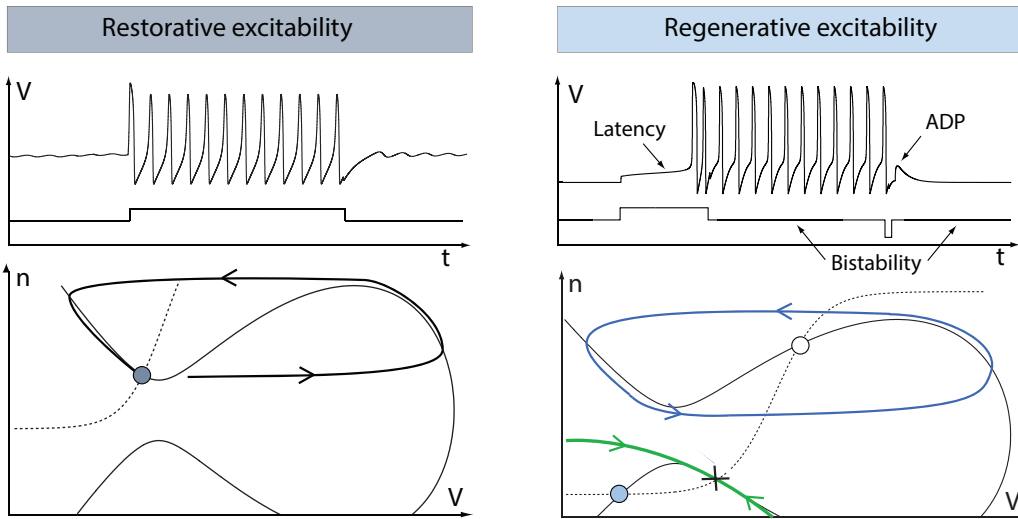


Figure 1. The bottom figures illustrate the typical phase portrait of restorative (left) and regenerative (right) excitability. The dark (resp. light) blue circle denotes a stable restorative (resp. regenerative) steady state (\bar{V}, \bar{n}) . The thin full (resp. dashed) line is the voltage (resp. slow variable) nullcline. The saddle point in the right phase portrait is represented as the cross and its separatrix as the green oriented line. The stable limit cycle surrounding the unstable fixed point (represented as a circle) is represented by the blue oriented line. The thick line in the left phase portrait represents the typical trajectory associated to the generation of an action potential. The top figures illustrate the typical accompanying electrophysiological responses to step variations of current.

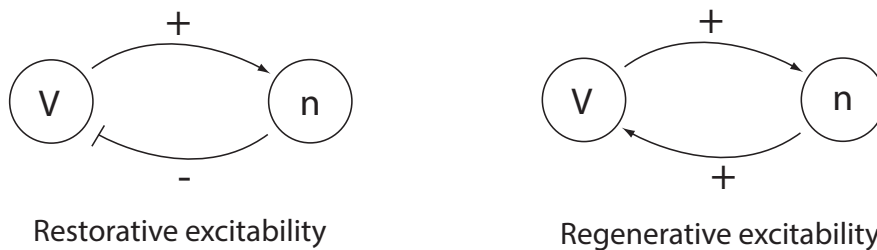


Figure 2. Block diagrams representation of restorative and regenerative excitability in planar models.

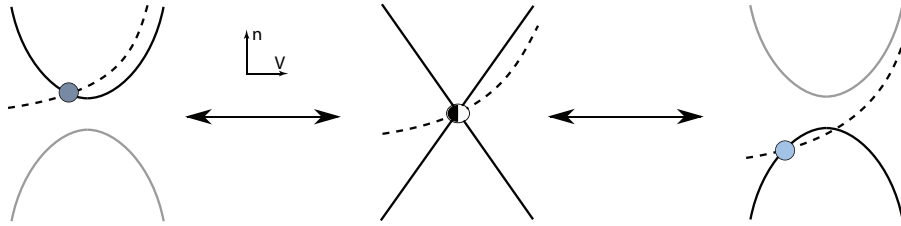


Figure 3. A continuous deformation from the restorative phase portrait of Fig. 1 left to the regenerative phase portrait of Fig. 1 right involving a transcritical bifurcation [17, Section 3.2] determined by the algebraic conditions (2) and (3). The dark blue circle represents a restorative stable steady-state, the light blue circle a regenerative stable steady-state, and the half-filled circle represents the transcritical bifurcation which separates the restorative and regenerative regimes.

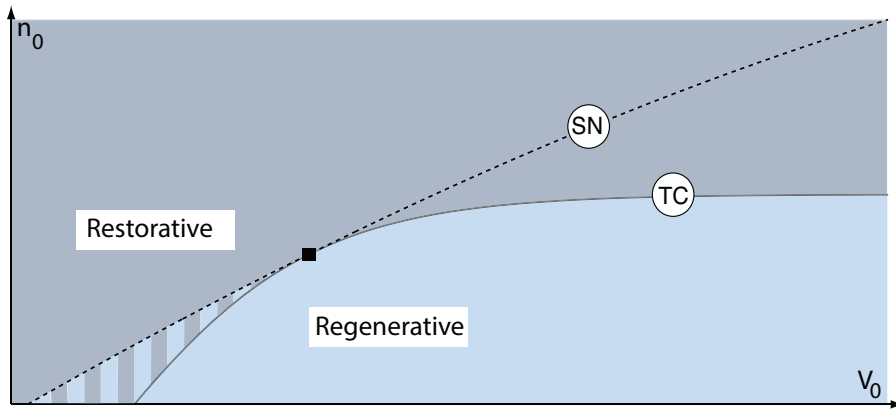


Figure 4. Excitability types in model (1). SN denotes the saddle-node bifurcation, TC the transcritical bifurcation. ■: Pitchfork bifurcation organizing center. Varying n_0 and V_0 the model switches between excitability types.

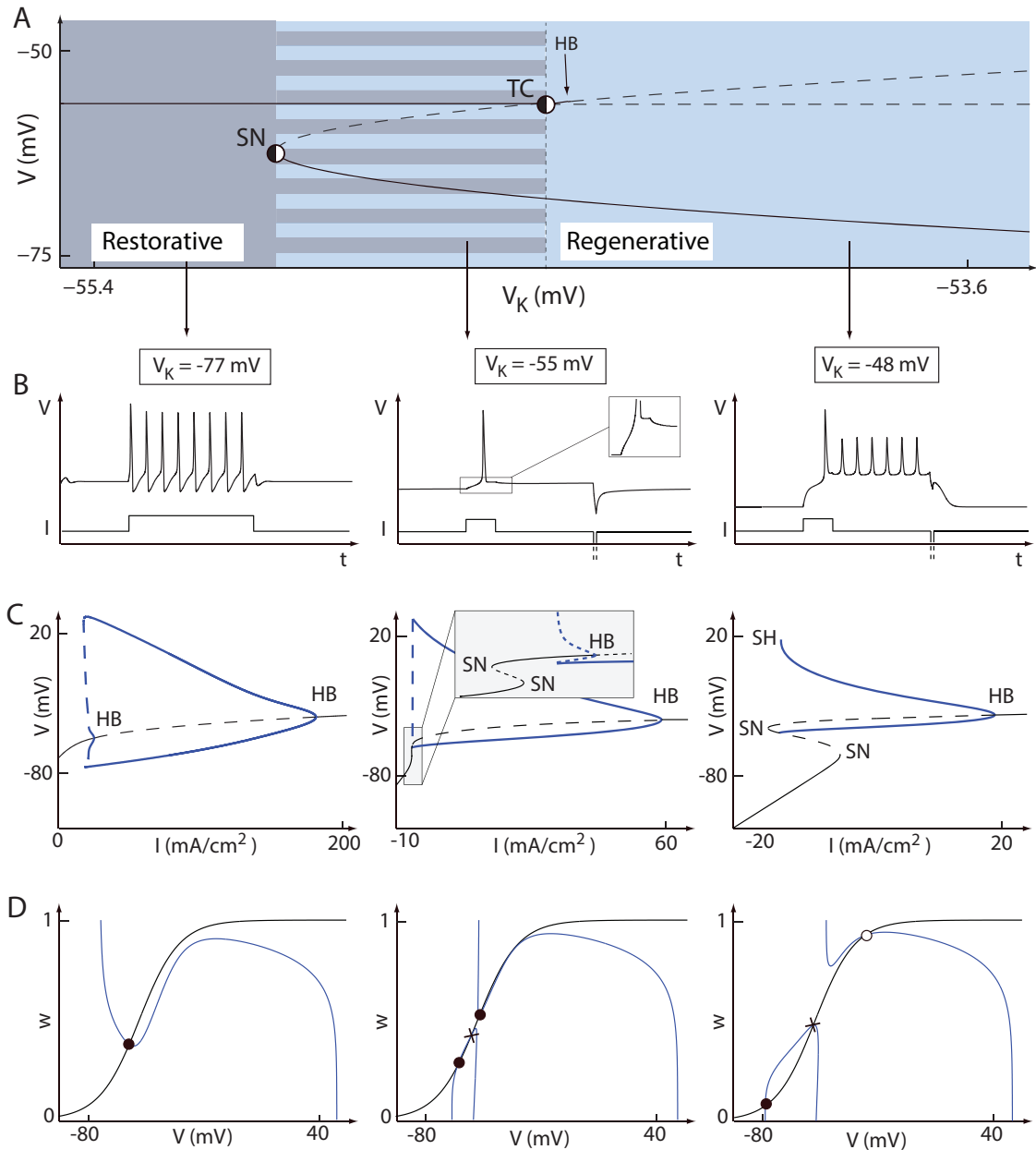


Figure 5. Variations of the potassium reversal potential V_K induce excitability switches in the Hodgkin-Huxley model. **A.** Bifurcation diagram of the HH model with V_K as the bifurcation parameter. TC denotes a transcritical bifurcation, SN a saddle-node bifurcation, HB a Hopf bifurcation. Branches of stable fixed points are represented as solid line, whereas branches of saddle points and unstable points as dashed lines. **B.** Electrophysiological responses of the model for three different values of V_K , corresponding to three different excitability types (restorative, mixed, and regenerative, from left to right). **C.** Bifurcation diagrams with the applied current as the bifurcation parameter for the same three values of V_K as in **B**. Black (resp. blue) full lines represent branches of stable steady-states (resp. limit cycles), black dashed lines branches of saddle and unstable steady-states. Branches of unstable limit cycle are drawn as dashed blue lines. HB denotes a Hopf bifurcation, SN a saddle-node bifurcation, and SH a saddle-homoclinic bifurcation. **D.** Phase portraits of reduced HH model proposed by Rinzel in [10] for the same three values of V_K as in **B,C**. Blue full lines denote the V -nullclines and black full lines the w -nullclines, where w denotes the slow variable of the reduced model. Filled circles denote stable steady-states, crosses saddle points, and circles unstable steady-states.

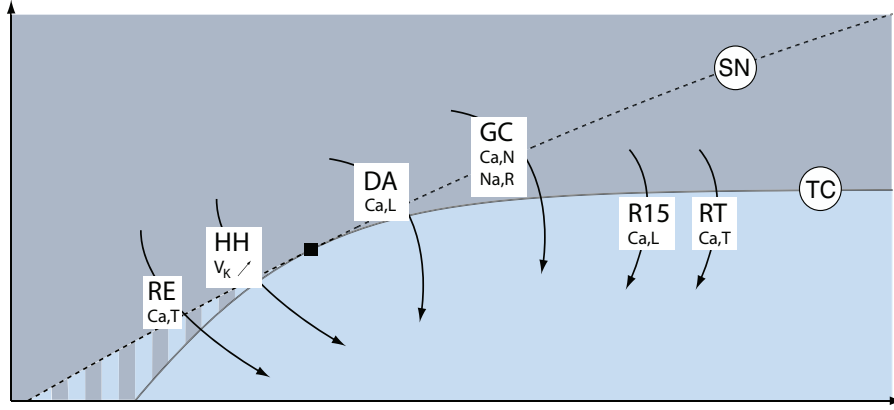


Figure 6. Modifications in the balance between restorative and regenerative channels induce excitability switches in conductance-based models. The figure sketches excitability switches of the Hodgkin-Huxley (HH) model [2], Aplysia's R15 neuron (R15) model [6], a dopaminergic (DA) neuron model [3], thalamic reticular (RT) and relay (RE) neuron models [4, 5], and a cerebral granule cell (GC) model [7] on the excitability parameter map computed for the two-dimensional model of [1]. All these conductance-based models can switch between restorative and regenerative excitability through the physiologically relevant regulation of specific ion channels.

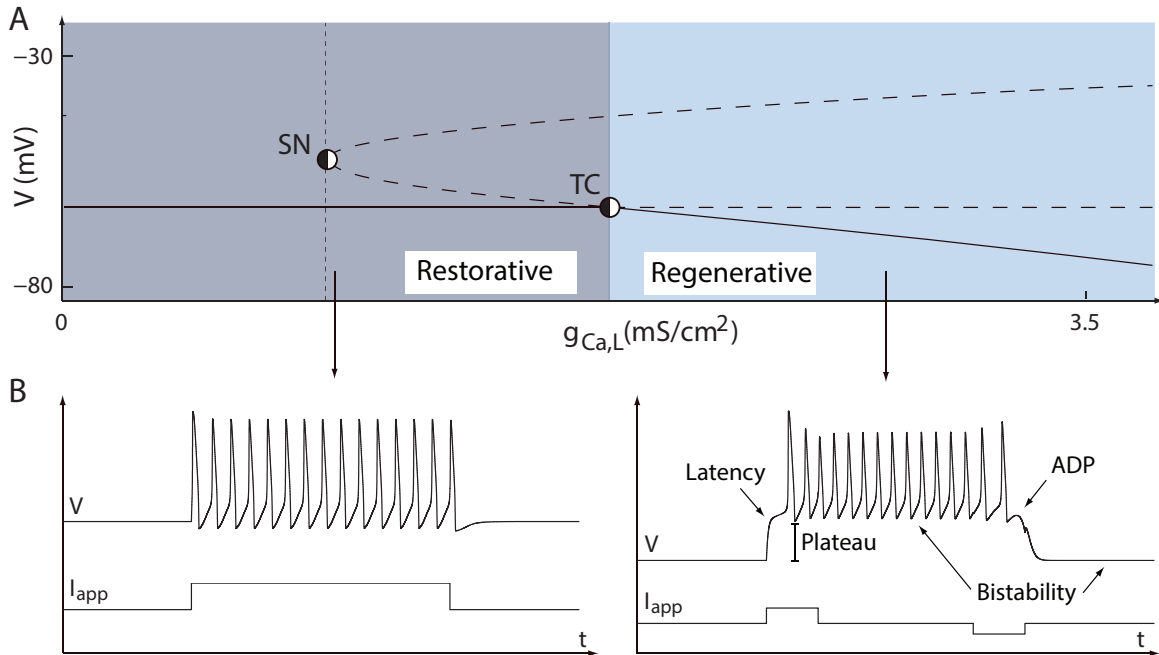


Figure 7. Variations of L-type calcium channel density $\bar{g}_{Ca,L}$ induce excitability switches in a model of DA neurons [3]. **A.** Bifurcation diagram of the model with $\bar{g}_{Ca,L}$ as the bifurcation parameter. TC denotes a transcritical bifurcation, SN a saddle-node bifurcation. Branches of stable fixed points are represented as solid line, branches of saddle points and unstable points as dashed lines. **B.** Electrophysiological responses of the model to step inputs of excitatory/inhibitory current (the intracellular calcium concentration is fixed at $[Ca^{2+}]_{in} = 300 \text{ nM}$, which is within the physiological range). For $\bar{g}_{Ca,L}$ lower (resp. higher) than the critical value $\bar{g}_{Ca,L}^c$, the model exhibits typical electrophysiological signature of restorative (resp. regenerative) excitability. The low $\bar{g}_{Ca,L}$ configuration corresponds to $\bar{g}_{Ca,L} = 1 \text{ mS/cm}^2$, whereas the high $\bar{g}_{Ca,L}$ configuration corresponds to $\bar{g}_{Ca,L} = 3 \text{ mS/cm}^2$.

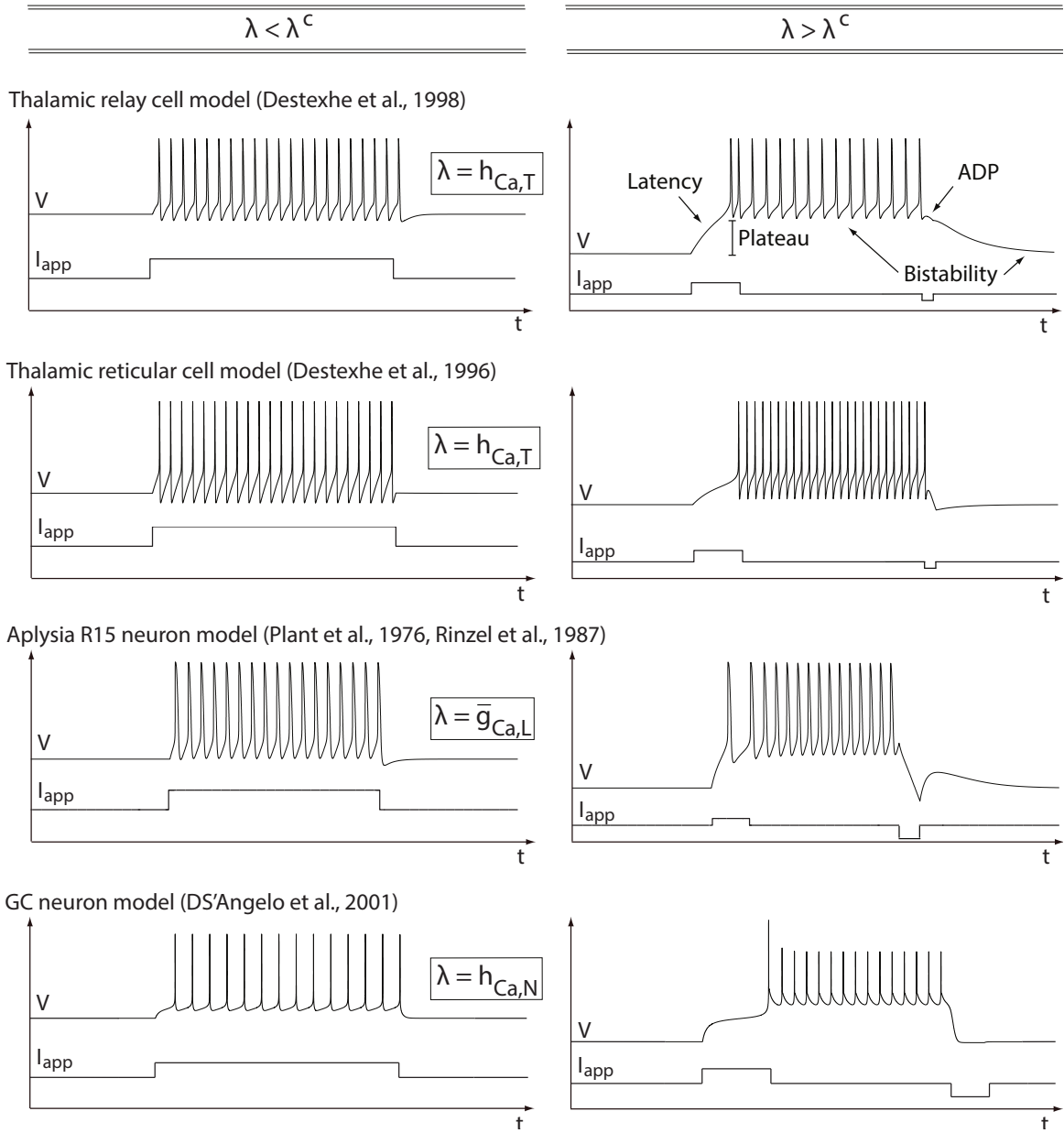


Figure 8. The same mathematical bifurcation in different conductance-based models causes the same switch in electrophysiological signatures. The figure shows the electrophysiological responses of various conductance-based models to step inputs of excitatory/inhibitory current when the bifurcation parameter λ is lower (left) or higher (right) than the critical value λ^c . This bifurcation parameter can be either the density or the inactivation variable of a regenerative channel. Other adaptation variables are set to constant values chosen in physiological ranges (see text). For λ lower (resp. higher) than the critical value λ^c , all models exhibit electrophysiological signatures of restorative (resp. regenerative) excitability. Numerical values of the parameter λ in the different plots are as follows. Thalamic relay cell: left $h_{Ca,T} = 0$, right $h_{Ca,T} = 0.2$. Thalamic reticular cell: left $h_{Ca,T} = 0$, right $h_{Ca,T} = 0.4$. Aplysia R15 neuron: left $\bar{g}_{Ca,L} = 10^{-6} mS/cm^2$, right $\bar{g}_{Ca,L} = 0.004 mS/cm^2$. GC neuron: left $h_{Ca,N} = 0.01$, $h_{Na,R} = 0.1$, right $h_{Ca,N} = 0.3$, $h_{Na,R} = 0.1$.

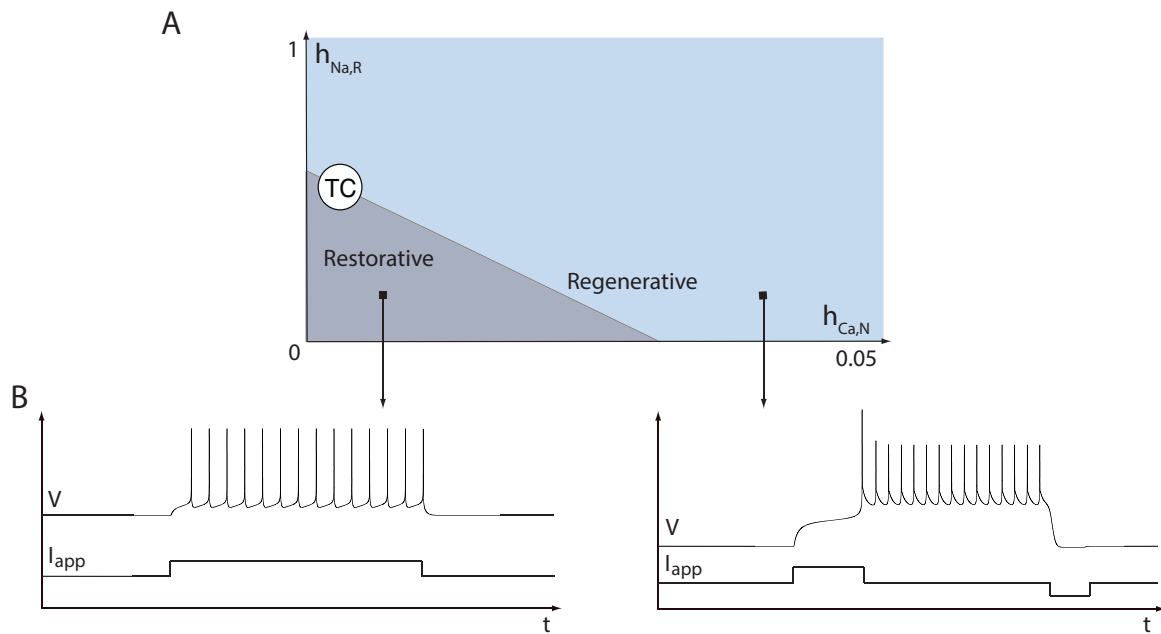


Figure 9. Joint variations of the inactivation gates of N -type calcium channels and resurgent sodium channels induce excitability switches in cerebellar granular cells. A. Two parameter bifurcation diagram of the mode with $h_{Ca,N}$ and $h_{Na,R}$ as bifurcation parameters. TC denotes a branch of transcritical bifurcations detected following the algorithm in Table 2. **B.** Electrophysiological responses of the model to step inputs of excitatory/inhibitory current: left $h_{Ca,N} = 0.01$, $h_{Na,R} = 0.1$, right $h_{Ca,N} = 0.3$, $h_{Na,R} = 0.1$.

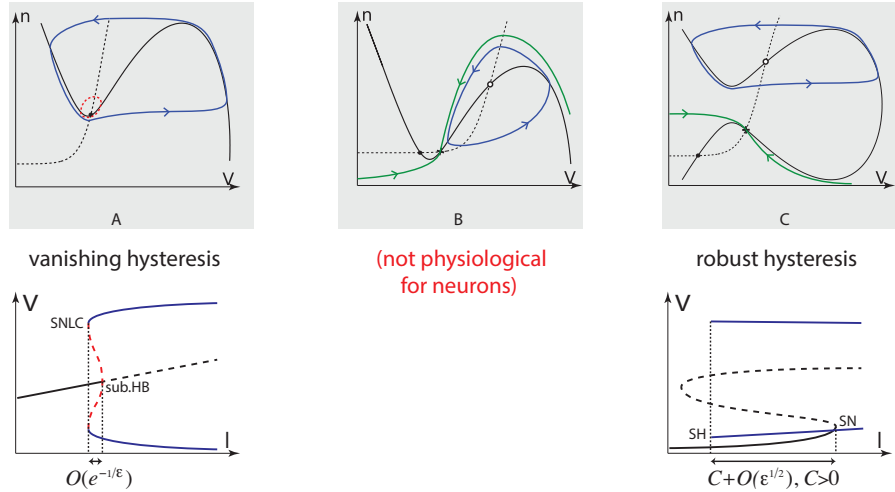


Figure 10. Three bistable phase portraits of model (1) and cartoon of the associated hysteretic bifurcation diagrams. In the phase portraits, a solid line denotes the V -nullcline, whereas a dashed line denotes the n -nullcline. Stable fixed points are depicted as filled circles, whereas unstable as circles and saddle points as cross. Stable limit cycles are drawn as solid oriented blue curves, whereas unstable as red dashed curves. The stable manifolds of saddle points are depicted as green oriented curves. In bifurcation diagrams, a solid line denotes branches of stable fixed points, whereas a dashed line denotes branches of unstable or saddle points. Branches of stable limit cycles are depicted as blue lines, whereas branches of unstable limit cycles as red dashed lines. *sub.HB* denotes a subcritical Hopf bifurcation, *SNLC* a saddle-node limit cycles bifurcation, *SN* a saddle-node bifurcation, and *SH* a saddle-homoclinic bifurcation.

A-B. Restorative bistability. **A.** Subcritical Hopf bifurcation. Hysteresis vanishes exponentially fast as timescale separation increases. **B.** Restorative saddle-homoclinic bifurcation. Not physiological because it violates the time scale separation between V and n .

C. Regenerative bistability ruled by a regenerative saddle-homoclinic bifurcation. Hysteresis is barely affected by time-scale separation.

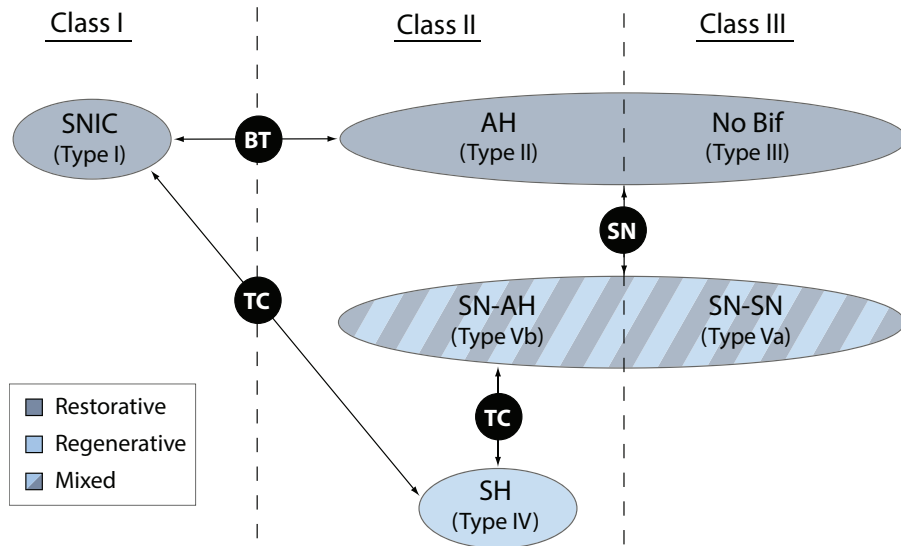


Figure 11. The various bifurcations associated to different types of neuronal excitability. *SNIC*: saddle-node on invariant circle; *BT*: Bogdanov-Takens; *AH*: Andronov-Hopf; *SN*: saddle-node; *TC*: transcritical; *SH*: saddle-homoclinic. See also [1] for more detailed definitions and properties of excitability Types I-V and associated transition bifurcations in a planar neuron model.

Class I excitability occurs in the neighborhood of a SNIC bifurcation [12] and is purely restorative.

Class II excitability can be either restorative in which case the stable equilibrium loses stability in a subcritical Hopf bifurcation (Type II in [12]) or regenerative in which case a stable equilibrium coexists with a stable limit cycle over a robust bistable range organized by a (singularly perturbed) saddle homoclinic bifurcation (Type IV in [1]). In a small parameter range, class II excitability can also exhibit a mixed type (Type Vb in [1]), where a regenerative "down" stable equilibrium coexists with a "up" restorative stable equilibrium or limit cycle. Stability of those attractors is lost either in saddle-node or Hopf bifurcations.

Class III excitability can be either restorative (a monostable equilibrium) or exhibits a mixed type (Type Va in [1]), where a regenerative down stable equilibrium coexists with a restorative up stable equilibrium. Both attractors lose stability in a saddle-node bifurcation.

The transition to regenerative excitability is always through a transcritical bifurcation.

Ion Channel	Gating Kinetics	Classification
Sodium Channels		
Transient	FA, SI - Negative feedback via SI	Slow restorative
Persistent	FA - No slow gating variable	Neutral
Resurgent	SA, USI - Positive feedback via SA	Slow regenerative
Calcium Channels		
L-type	SA - Positive feedback via SA	Slow regenerative
T-type	SA, USI - Positive feedback via SA	Slow regenerative
N, P/Q, R-type	SA, USI - Positive feedback via SA	Slow regenerative
Potassium Channels		
Delayed Rectifiers	SA - Negative feedback via SA	Slow restorative
KCNQ	USA - No slow gating variable	Neutral
eag/erg	USA - No slow gating variable	Neutral
A-type	FA, SI - Positive feedback via SI	Slow regenerative
BK	SA - Negative feedback via SA	Slow restorative
HCN	SA - Negative feedback via SA	Slow restorative

FA: fast activation, FI: fast inactivation, SA: slow activation, SI: slow inactivation, USA: ultraslow activation, USI: ultraslow inactivation

Table 1. Classification of ion channels according to their gating kinetics. Activation and inactivation variables are distributed in three groups: fast, slow, and ultra-slow (adaptation). Slow variables are defined as restorative (resp. regenerative) if they induce a negative (resp. positive) feedback on membrane potential variations. An ion channel that possesses a slow restorative variable is called “slow restorative channel”, and similarly for slow regenerative channels. Channels that do not possess a slow variable are called “neutral channels”. This classification might change for a given channel for some channel subtypes.

Algorithm for the detection of a transcritical bifurcation in generic conductance-based models via modulation of a regenerative ionic current and computation of the excitability switch bifurcation diagram.

<p>(i) Classification of gating variables as fast (\mathcal{G}_F), slow (\mathcal{G}_S), and adaptation (\mathcal{G}_A) variables</p> <p>(i-a) Following Tab. 1, group gating variables in the three groups \mathcal{G}_F, \mathcal{G}_S, and \mathcal{G}_A.</p> <p>(i-b) Split \mathcal{G}_S in regenerative $\mathcal{G}_{S,+}$ and restorative $\mathcal{G}_{S,-}$ slow gating variables.</p> <p>(i-c) If adaptation variables are present, set them to constant physiologically relevant values.</p>
<p>(ii) Balance equation and choice of the bifurcation parameter</p> <p>(ii-a) Select a regenerative ionic current I_{reg} and the associated regenerative slow gating variable x^{reg}.</p> <p>(ii-b) Write the balance equation</p> $\left. \frac{\partial \dot{V}}{\partial x^{reg}} \frac{\partial x_{\infty}^{reg}}{\partial V} \right _{TC} = - \sum_{x^{r-}} \overbrace{\left. \frac{\partial \dot{V}}{\partial x^{s-}} \frac{\partial x_{\infty}^{s-}}{\partial V} \right _{TC}}^{< 0} - \sum_{x^{s+} \neq x^{reg}} \overbrace{\left. \frac{\partial \dot{V}}{\partial x^{s+}} \frac{\partial x_{\infty}^{s+}}{\partial V} \right _{TC}}^{> 0} \quad (\text{b.eq.})$ <p>(ii-c) If I_{reg} has an adaptation variable x^a, pick it as the bifurcation parameter λ regulating the left hand side of (b.eq.), that is $\lambda = x^a$.</p> <p>If I_{reg} has no adaptation variable, pick $\lambda = \bar{g}_{reg}$.</p>
<p>(iii) Singularity condition and fixed point equation</p> <p>(iii-a) Solve (b.eq.) together with the singularity condition (8), in V and λ.</p> <p>For numerical implementation, recall that the left hand side of (8) is proportional to</p> $\frac{\partial \dot{V}}{\partial V} + \sum_{x^f} \frac{\partial \dot{V}}{\partial x^f} \frac{\partial x_{\infty}^f}{\partial V}$ <p>(iii-b) Plug the computed values V^c and λ^c into the fixed point equation $\dot{V} _{TC} = 0$ to compute the value of the applied current at the transcritical bifurcation (I^c).</p>
<p>(iv) Tracking of excitability switches</p> <p>Change the applied current according to the equation</p> $I_{app} = I^c - \left. \frac{\partial \dot{V}}{\partial \lambda} \right _{TC} (\lambda - \lambda^c),$ <p>and compute the model bifurcation diagram with V as the variable and λ as the bifurcation parameter.</p>

Table 2

Supplementary material

Construction of the transcritical bifurcation in generic conductance-based models

Suppose that, given a bifurcation parameter $\mu \in \{\bar{g}_i, E_i\}_{i \in \mathcal{I}}$, there exists a solution $(V, \mu) = (V_{TC}, \mu_{TC})$ satisfying the two degeneracy conditions (7) and (8). Then we claim that, posing

$$I_{TC} = \sum_i \bar{g}_i m_{i\infty}^{a_i}(V_{TC}) h_{i\infty}^{b_i}(V_{TC}) (V_{TC} - E_i),$$

which solves the fixed point equation, the model is at a transcritical bifurcation. The existence of the couple (V_{TC}, μ_{TC}) in the physiological range is shown for specific examples in the main document.

The center space E_c associated to the degeneracy conditions (7) and (8) is spanned by the vector

$$v_c = (1, \mathbf{k}), \quad \mathbf{k} := [k_x]_x, \quad k_x := \left. \frac{\partial x_\infty}{\partial V} \right|_{V=V_{TC}},$$

where x runs all fast and recover gating variables in the model, that is \mathbf{k} is the vector whose elements are the slopes of the (in)activation functions of all the fast and recovery gating variables calculated at $V = V_{TC}$. The associated center manifold \mathcal{M}_c is exponentially attractive. Indeed, it can easily be shown that, when (7) and (8) are satisfied, the remaining nonzero eigenvalues of the Jacobian of (10) are all negative. To the first order, the dynamics on \mathcal{M}_c is given by

$$C_m \dot{V}_c = - \sum_{i \in \mathcal{I}} \bar{g}_i (m_{i,\infty}(V_{TC}) + k_{m_i}(V_c - V_{TC}))^{a_i} (h_{i,\infty}(V_{TC}) + k_{h_i}(V_c - V_{TC}))^{b_i} (V_c - E_i) + I_{app}$$

Consider the affine reparametrization

$$\tilde{\mu} = \mu, \quad \tilde{I}_{app} = I_{app} + \left. \frac{\partial \dot{V}_c}{\partial \mu} \right|_{\substack{\mu=\mu_{TC} \\ V=V_{TC}}} (\mu - \mu_{TC}). \quad (\text{S16})$$

It is easy to show that, in the affine reparametrization (S16), the center manifold dynamics satisfy

$$\dot{V}_c = \left. \frac{\partial \dot{V}_c}{\partial V} \right|_{\substack{\mu=\mu_{TC} \\ V=V_{TC}}} = \left. \frac{\partial \dot{V}_c}{\partial \tilde{\mu}} \right|_{\substack{\mu=\mu_{TC} \\ V=V_{TC}}} = 0$$

corresponding to the defining condition of a transcritical bifurcation (see [1, Page 367]).

Supplementary references

- [1] Seydel R (2010) Practical bifurcation and stability analysis, volume 5 of Interdisciplinary Applied Mathematics. New York: Springer-Verlag, third edition.